Statistics of charge collection in liquid argon and liquid xenon

J. Thomas and D. A. Imel
Norman Bridge Laboratory of Physics, 161-33, California Institute of Technology, Pasadena, California 91125

S. Biller
Department of Physics, University of California, Irvine, California 92717
(Received 30 September 1987)

There is a fundamental limit to the resolution that can be achieved in liquid-argon and liquid-xenon ionization detectors due to statistical fluctuations in the rate of charge collection along the track of a primary particle. The limit is typically much larger than the resolution expected from Poisson statistics. We present resolution data in both argon and xenon, a model to describe the data, and a discussion of how the model parameters can be manipulated in order to achieve even greater resolution.

I. INTRODUCTION

It is the purpose of this paper to show that charge density fluctuations caused by the statistics of δ electron production affect the energy resolution observed in liquid argon and liquid xenon ionization detectors. We will do this using a model of charge collection that is based on a more realistic description of liquid noble gases than either the Onsager theory[1] or the Jaffe-Kramers columnar recombination theory.[2,3]

Liquid xenon and liquid argon are remarkable media because the energy required to form an ion electron pair is small, 15.6 and 23.6 eV, respectively.[4] The statistical fluctuation in these numbers is small due to the unique solid-state properties of argon and xenon.[5] (We assume that liquid properties are closely related to the solid-state properties.) One way to express the statistical variation in the ionization process is through the Fano factor,[6]

$$\sigma = \sqrt{FE_p W}\,, \tag{1}$$

where σ is the variance of the energy signal, F is the Fano factor, E_p the energy of the primary particle, and W is the energy required to form an ion electron pair. The Fano factor is an expression of the deviation of the ionization process away from independent, identically distributed ionization events. For a Poisson process $F=1$, but if all ionization events are identical $F=0$. The Fano factor in xenon is 0.06 and in argon it is 0.12.[7] This is due to the small number of degrees of freedom for the deexcitation of energetic electrons and the small band gap in these materials, 9.3 eV in xenon and 14.3 eV in argon.[5,7,8]

Extremely good energy resolution in liquid argon or xenon should be possible. Estimates based on the Fano factor go as low as 0.4% full width at half maximum (FWHM) at 1 MeV in argon.[8] But only ≈3% resolution has been observed in liquid argon even at extremely high electric fields.[9–12] What is the mechanism that accounts for this? It is probably not electronegative impurities. The liquid argon and liquid xenon used in these experiments had impurity concentrations near one part per billion oxygen equivalent. This corresponds to an electron drift attenuation length of 150 cm (Ref. 13) at 1 kV/cm and the detectors were only a few centimeters long. Even the finite range of the electron from a conversion source does not enter in a significant way at these impurity levels. It would take concentrations of the order of 100 ppb before the emission of an electron parallel to the cathode would differ, at the few percent level, from the collected charge from an electron emitted perpendicular to the cathode.

It is possible that all of the experiments in liquid argon were poorly designed. But these and other groups have consistently reported the same results with different apparatus. (The experimental data in liquid xenon is not as consistent.) We believe, instead, that the poor results are due to intrinsic charge-density fluctuations along the path of an ionizing particle[14] since these fluctuations affect the rate of recombination of the electron-ion pairs.

It is well known that charge-density fluctuations exist along the track of an ionizing particle. Figure 1 shows an electron traveling through a time projection chamber filled with two atmospheres of argon.[15] As the particle slows down it loses energy at a relatively fixed rate until it becomes nonrelativistic. At about this time, the energy loss increases and the particle loses the remainder of its energy in a relatively short distance (see Fig. 2). The high charge deposition region, or blob, at the end of the track represents an energy loss of 30–40 keV.[16]

We will begin with a simple single charge-density model to demonstrate that the charge-density fluctuations shown in Fig. 1 affect the observed resolution. Later, we will build a double charge-density model.

In a previous paper,[17] we showed that the charge collected in liquid argon or xenon is given by the expression

$$\frac{Q}{Q_{\max}} = \frac{\ln(1+\xi)}{\xi}, \tag{2}$$

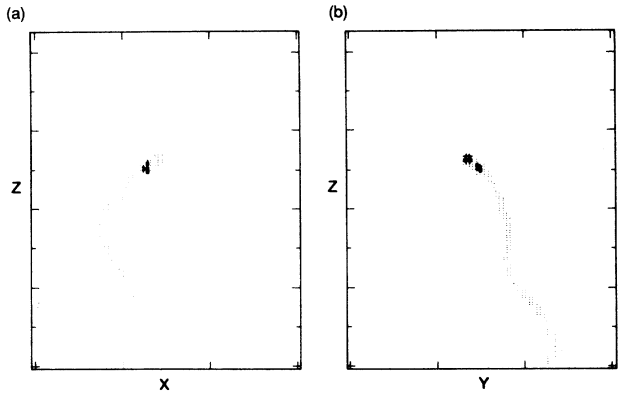

FIG. 1. (a) $X-Z$ and (b) $Y-Z$ projections of an electron track as it passes into a time projection chamber filled with 2 atmospheres of argon-methane (90/10 mixture). The electron stops near the center of the chamber and deposits 30-40 keV of energy in a well-localized "blob." The X and Y axes are 30 cm wide and the Z axis is scaled accordingly (see Ref. 15).

where $\xi = N_0\alpha/4a^2u\_E$, E is the magnitude of the electric field, $u\_$ the electron mobility, N_0 the charge per unit cell of dimension a, and α a phenomenological recombination coefficient.

This single density model of charge collection is based on more physically realistic assumptions about liquid noble gases than either the Onsager[1] or the Jaffe-Kramers[2,3] theories. The fact that the Onsager and Jaffe-Kramers theories may not be applicable in liquid noble gases has been noted by other authors[4,18] and the limitations have been discussed in our previous paper. Briefly, the Onsager model assumes that the electrons and ions interact via an infinite range coulomb potential. But in liquid noble gases the high coefficient of polarization for the medium causes the induced dipole moments to reduce the effective charge of an ion within a few atomic spacings.[5] The resulting polarization potential falls off more quickly than $1/r$ and, in argon, is so deep that the ions travel by quantum assisted tunneling.[19,20] Consequently, the ion mobility is several orders of magnitude smaller than the electron mobility.[21] It is not surprising, then, that the Onsager theory has difficulties describing the rate of recombination in liquid argon and liquid xenon.

The Jaffe-Kramers theory of columnar recombination assumes that the electron and ion mobilities are equal. In addition, it assumes that the ion-electron pairs are distributed in a uniform column of charge so that the drifting electrons and ions pass through neighboring charge distributions on their way to the anode and cathode. These columnar boundary conditions cannot be justified in liquid argon, for example, since the secondary electron interaction sites are separated by an average distance of ~ 100 atomic spacings.

Our single density model, Eq. (2), assumes that the individual ion-electron pairs are well separated (geminate theory) and also assumes that the positive ion mobility is several orders of magnitude smaller than the electron mobility. We have already shown[17] that it provides a good description of charge collection in liquid argon but we did not discuss the observed energy resolution. In the rest of this paper, we will try to create a realistic model that describes the energy resolution.

The single density model neglects the effects of charge density fluctuations along the track of the primary particle. A simple way to describe the effect of the fluctuations on the energy resolution is to take the derivative of Eq. (2) with respect to N to find

$$\frac{dQ}{Q} = \frac{dN}{N}\frac{\left|\frac{\ln(1+\xi)}{\xi} - \frac{1}{1+\xi}\right|}{\frac{\ln(1+\xi)}{\xi}}. \tag{3}$$

A fit of this equation to an independent data set[12] is shown in Fig. 3 where we have assumed that the width of the peaks $W_{\mathrm{FWHM}} = D\,dQ/Q$. The proportionality constant, D, may depend on the energy of the incident particle and the characteristics of the medium. A reasonable description of the data is achieved if $\xi E = 0.80$, a value fixed by the charge collection data alone, and $D\,dN/N = 0.51$. (In our previous paper,[12] we recom-

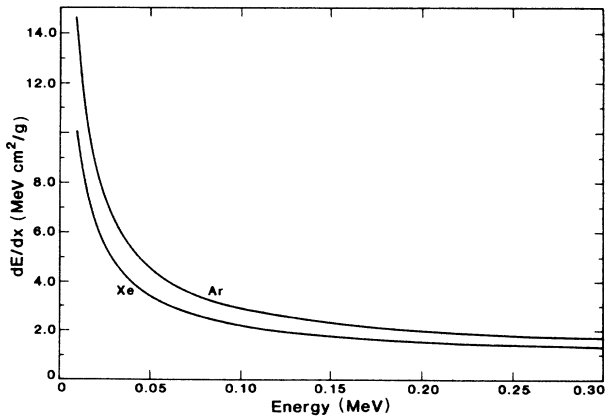

FIG. 2. Energy loss for electrons in argon and xenon as a function of energy. Note the rapid increase in dE/dx below 50 keV (Ref. 24).

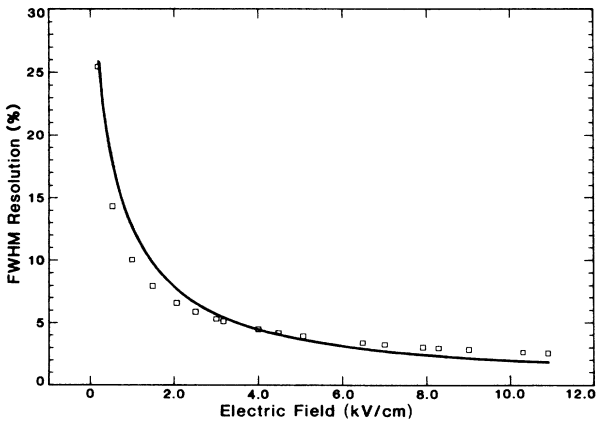

FIG. 3. A fit of Eq. (3) to the measured resolution of a 976-keV electron in liquid argon (Ref 12).

mended that $\xi E = 0.84$ for liquid argon although $\xi E = 0.80 \pm 0.02$ is better when the fit includes several data sets that were not evaluated in that publication. Our best estimate of ξE is sensitive to the absolute calibration of the charge collection data and since the existing data typically have a systematic uncertainty of $\pm 5\%$ it is obvious that more precise data would be desirable.)

We will generalize this single charge-density model in the next section, compare it to experimental data, and conclude with a discussion of how the model parameters can be manipulated in order to achieve even greater resolution than has already been obtained.

II. δ ELECTRON PRODUCTION AND THE STATISTICS OF CHARGE COLLECTION

The effect of charge-density fluctuations on the resolution of liquid noble gas ionization detectors has been discussed in the literature[22] but only in the context of the Jaffe-Kramers theory. We will show that a fundamental limit to the resolution comes naturally from our more physically realistic model of charge collection.

A simple description of the δ electron production process is provided by the Rutherford scattering cross section. For nonrelativistic δ electrons (the primary may be relativistic) and for small scattering angles, the momentum transferred to the δ electron is $p_\delta = p\theta$, where p is the momentum of the primary electron. The probability of scattering a δ electron of energy E_δ from a target of thickness Δx g/cm^2 is[23]

$$P(E_\delta)\, dE_\delta = \frac{2\pi N_A e^4}{\beta^2 m_e c^2} \frac{Z}{A} \Delta x \frac{dE_\delta}{E_\delta^2}, \tag{4}$$

where Z is the atomic number of the target, A its atomic mass, m_e and e the mass and charge of an electron, and N_A is Avogadro's number. Equation (4) is valid for a broad range of δ electron energies and will fail only when the scattering angle of the δ electron is large ($\gtrsim 1$ rad). This expression is also valid for a broad range of primary electron energies and should fail only if the primary electron energy is small ($\lesssim$ 1keV) where it is important that the scattering electron is bound rather than free.

Equation (4) is more easily expressed in terms of the energy loss of the primary electron. We use the expressions compiled by Pages *et al.*[24] for the energy loss due to ionization

$$\frac{dE}{dx} = \frac{2\pi N_A e^4}{\beta^2 m_e c^2} \frac{Z}{A} \times \left[\ln \frac{T^2(T+2)}{2I^2} + \frac{T^2/8 - (2T+1)\ln(2)}{(T+1)^2} + 1 - \beta^2 \right], \tag{5}$$

where $T = E/m_e c^2$ and I is the mean excitation energy of the target in units of $m_e c^2$; $I\, m_e c^2 \approx 9.73Z + 58.8Z^{-0.19}$ eV.

The number of δ electrons of energy E_δ produced by a primary electron, $N(E_p, E_\delta)$, can be calculated by integrating $P(E_\delta)$ from 0 to E_p and utilizing equation (5). Then,

$$N(E_p, E_\delta) = F(E_p) \frac{dE_\delta}{E_\delta^2}, \tag{6}$$

where

$$F(E_p) = \int_0^{E_p} dE \left[\ln \frac{T^2(T+2)}{2I^2} + \frac{T^2/8 - (2T+1)\ln(2)}{(T+1)^2} + 1 - \beta^2 \right]^{-1} \tag{7}$$

can be evaluated numerically and is shown in Fig. 4 as a function of energy in xenon and argon. $F(E_p)$ is a smooth function of energy and approximate expressions for F are

$$F_{\mathrm{Ar}}(E_p) = -4.00\times 10^{-6} E_p^2 + 6.80\times 10^{-2} E_p + 2.83, \tag{8a}$$

$$F_{\mathrm{Xe}}(E_p) = -5.12\times 10^{-6} E_p^2 + 7.84\times 10^{-2} E_p + 4.28. \tag{8b}$$

An interesting consequence of Eq. (6) is that the energy carried by the δ electrons, NE_δ, in a interval dE_δ, is proportional to $1/E_\delta$ and the fluctuation in the total energy, $E_\delta\sqrt{N}$, is a constant. Therefore the effect of the high-energy δ electrons is as important as the more abundant low-energy δ electrons in determining the resolution of an ionization detector.

The δ electrons should in principle carry away all of the energy of the primary electron. But since each high-energy δ electron can produce lower-energy δ electrons, and so on, the distribution of energies predicted by Eq. (6) should be weighted more heavily toward lower energies. This does not represent a large perturbation since

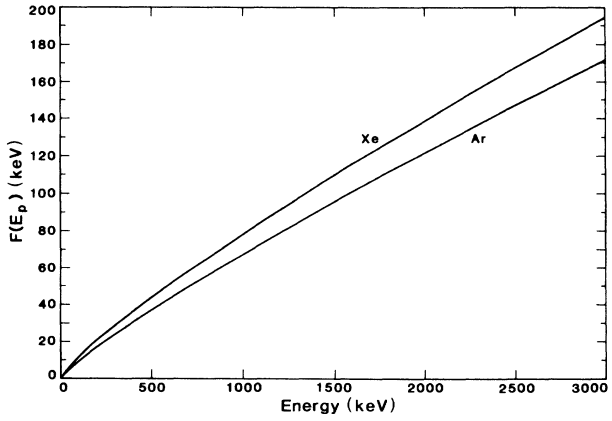

FIG. 4. The function $F(E_p)$, defined by Eq. (7), is essentially linear. Second-order fits to these curves are listed in Eq. (8).

the probability of a high-energy δ electron on a still higher-energy δ electron depends on the product of two small probabilities. We approximate these second-order effects by normalizing the integral over all δ electron energies to the energy of the primary particle,

$$E_p \equiv F(E_p)\int_{E_0}^{E_p}\frac{dE_\delta}{E_\delta^2}E_\delta = F(E_p)\ln\left[\frac{E_p}{E_0}\right]. \quad (9)$$

E_0 represents the minimum kinetic energy of a secondary electron and should be near the ionization energy of the atom since this is where the Rutherford scattering cross section breaks down. We define E_0 such that Eq. (9) is true and use this result to normalize the secondary electron distributions in the work that follows. (For the case of a 368-keV primary electron in xenon, $E_0 = 4.2$ eV.)

We will use a simple double density model to describe the charge-density fluctuations. Along the minimum ionizing part of an electron track the charge density is described by the parameter ξ_1 and near the end of the electrons range, where dE/dx increases dramatically, the charge density is described by ξ_0. Thus every high-energy δ electron track has a minimum ionizing portion and a high charge-density blob at its endpoint. The total charge collected from these two regions will be different and we can modify Eq. (9) to take this into account. The number of δ electrons in a given energy interval is dE_δ/E_δ^2 and the energy collected from the δ electrons is $E_\delta\,[\ln(1+\xi)]/\xi$. Being careful to normalize the δ electron distribution we find that the collected energy, E_c, is

$$\frac{E_c}{E_p} = \left[\int_{E_0}^{E_1}\frac{dE_\delta}{E_\delta^2}E_\delta\frac{\ln(1+\xi_1)}{\xi_1} + \int_{E_1}^{E_2}\frac{dE_\delta}{E_\delta^2}E_\delta\frac{\ln(1+\xi_0)}{\xi_0} + \int_{E_2}^{E_p}\frac{dE_\delta}{E_\delta^2}E_2\frac{\ln(1+\xi_0)}{\xi_0} + \int_{E_2}^{E_p}\frac{dE_\delta}{E_\delta^2}(E_\delta - E_2)\frac{\ln(1+\xi_1)}{\xi_1}\right]\left[\int_{E_0}^{E_p}\frac{dE_\delta}{E_\delta^2}E_\delta\right]^{-1}. \quad (10)$$

Those δ electrons with energies lower than E_1 do not produce a high charge-density blob; there are simply too few electron-ion pairs created (at a cost of ≈25 eV per pair). δ electrons with energies between E_1 and E_2 go entirely into a high charge-density blob. And δ electrons with energies above E_2 expend part of their energy along a minimum ionizing track and the remainder in a high-density blob.

It is trivial to show that Eq. (10) reduces to

$$\frac{E_c}{E_p} = \left[a\frac{\ln(1+\xi_0)}{\xi_0} + (1-a)\frac{\ln(1+\xi_1)}{\xi_1}\right], \quad (11)$$

where

$$a \equiv \left[\frac{\ln\left[\frac{E_2}{E_1}\right] - \frac{E_2}{E_p} + 1}{\ln\left[\frac{E_p}{E_0}\right]}\right].$$

Thus in the limit of small charge-density fluctuations, we recover Eq. (2).

This model leads to a finite resolution effect in liquid argon that is larger than the Fano factor limited resolution and should be added in quadrature to it. The effect follows from Eq. (6) which predicts $N(E_p,E_\delta)$ δ electrons of energy E_δ with a variance $\sqrt{N(E_p,E_\delta)}$. But since the fluctuation in collected energy due to the blob is proportional to the difference in charge collected from the track and the blob, the variance in the observed energy signal is

$$\sigma^2 = \sum N(E_p,E_\delta)E_\delta^2\left[\frac{\ln(1+\xi_1)}{\xi_1} - \frac{\ln(1+\xi_0)}{\xi_0}\right]^2.$$

The total variance is the sum, in quadrature, over all δ electron energies that are high enough to create a charged blob. [See the second and third terms in Eq. (10).] To be more specific, our model is

$$\frac{\sigma^2}{E_c^2} = \left[F(E_p)\ln^2\left[\frac{E_p}{E_0}\right]\frac{E_c^2}{E_p^2}\right]^{-1}\left[\int_{E_1}^{E_2}\frac{dE_\delta}{E_\delta^2}E_\delta^2\left[\frac{\ln(1+\xi_1)}{\xi_1} - \frac{\ln(1+\xi_0)}{\xi_0}\right]^2 + \int_{E_2}^{E_p}\frac{dE_\delta}{E_\delta^2}E_2^2\left[\frac{\ln(1+\xi_1)}{\xi_1} - \frac{\ln(1+\xi_0)}{\xi_0}\right]^2\right], \quad (12)$$

which reduces to a simple expression for the observed width of a peak in a spectrum:

$$W_{\mathrm{FWHM}}(\%) = \frac{235.5\left[F(E_p)\left[2E_2 - E_1 - \frac{E_2^2}{E_p}\right]\right]^{1/2}}{F(E_p)\ln\left[\frac{E_p}{E_0}\right]\frac{E_c}{E_p}} \times \left[\frac{\ln(1+\xi_1)}{\xi_1} - \frac{\ln(1+\xi_0)}{\xi_0}\right]. \quad (13)$$

In the limit of small charge fluctuations, it can be shown that Eq. (13) reduces to Eq. (3) if

$$D\frac{dN}{N} = \frac{235.5}{E_p}\left[F(E_p)\left[2E_2 - E_1 - \frac{E_2^2}{E_p}\right]\right]^{1/2}.$$

But now it is possible to model the situation where the charge density fluctuations are not small and we have an explicit prediction of how $D\ dN/N$ varies with the energy of the primary particle. In leading order, the percent energy resolution varies as $E_p^{-1/2}$.

Equations (11) and (13) can be tested against experimental data. Figures 5, 6, and 7 present our model versus the liquid argon data collected by Imel[25], Scalettar[26] and Aprile[12]. In Imel's and Aprile's data sets, the O_2 impurity concentrations were ≈ 1 ppb and so do not affect the resolution in the small chambers used for these studies except at very low fields (< 100 V/cm). Scalettar's data was collected in a large ionization chamber equipped with a movable cathode so that the exponential attenuation of the collected charge, due to the impurities, could be measured directly. So the data presented in Fig. 7 has had the effect of the impurities removed, for all field

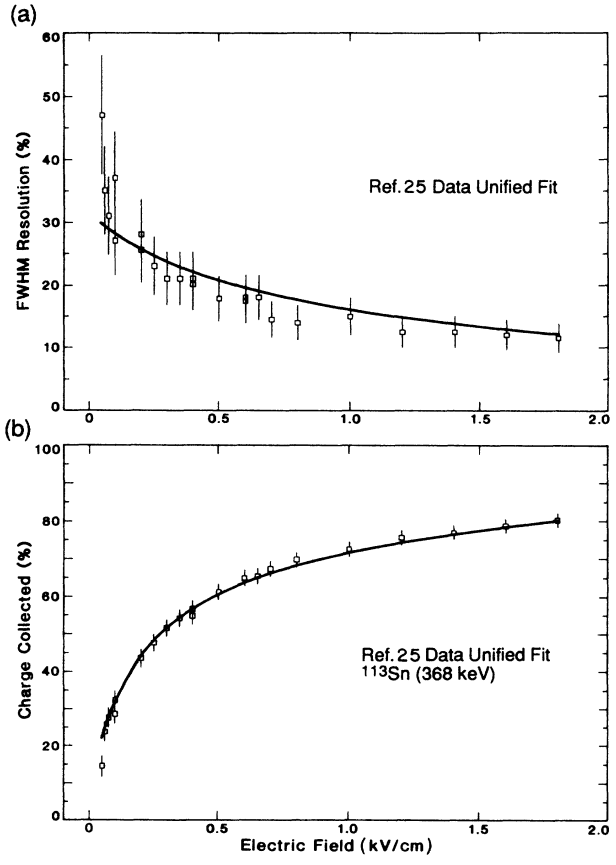

FIG. 5. A simultaneous fit of Eqs. (11) and (13) to the (a) energy resolution and (b) charge collected in liquid argon (Ref. 25). The data shown in Figs. 7 and 8 were fit at the same time. (FWHM error bars are shown.)

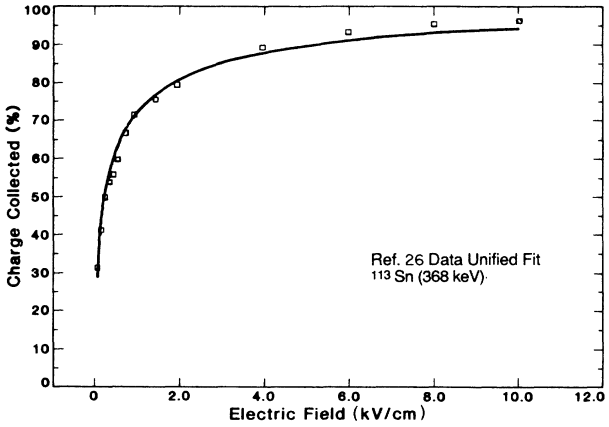

FIG. 6. The unified fit of Eq. (11) compared to the data in Ref. 26.

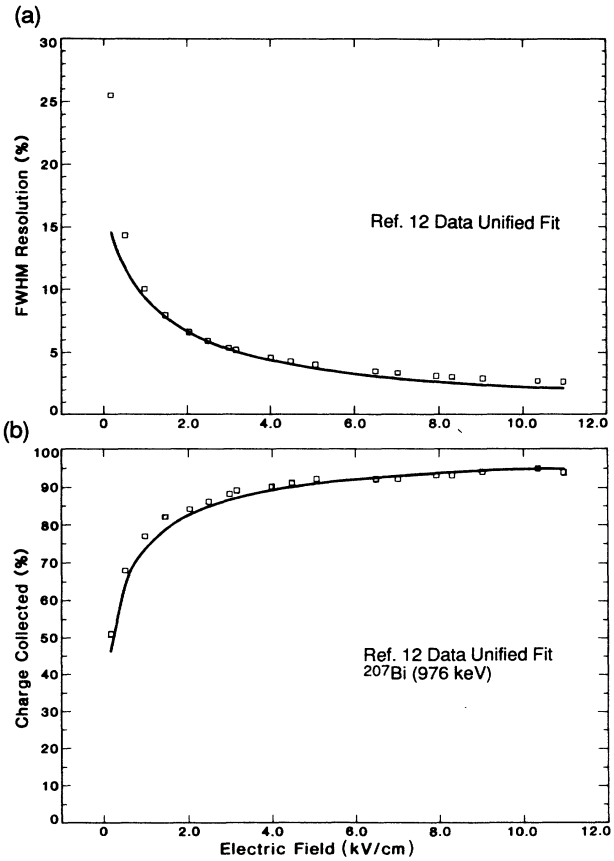

FIG. 7. The unified fit of Eqs. (11) and (13) compared to the data in Ref. 12.

strengths, and this was the data set used to determine ξE in our previous paper.[17]

The double density model was fit to the data in the following way: the charge collection data sets by Imel[25], Scalettar[26], and Aprile[12] were fit simultaneously with the resolution data sets collected by Imel[25] and Aprile[12]. (Scalettars[26] publication unfortunately does not include resolution results.) Imel's and Scalettars's data were collected using a ^{113}Sn source which emits 368-keV conversion electrons. Aprile's data were collected using the 976-keV conversion electrons from a ^{207}Bi source. The errors on Scalettar's and Aprile's data were not published and so we assumed that all three data sets are subject to the same errors for the purpose of the fitting procedure. Also, all of the charge collection data sets were subject to a 5% systematic uncertainty in the calibration of the electronics. We have taken Imel's and Aprile's data as is, without normalization. Scalettar's data were systematically high in all of the fits and so we reduced his normalization by 2% ($\approx\frac{1}{2}\sigma$) in order to get the best understanding of the shapes of the curves. Thus, the normalizations were fixed and not fit. The resolution data are relative data and so there is no systematic uncertainty in the magnitude of these values.

A unified fit to all five data sets yields $\xi_1 E = 0.34 \pm 0.12$, $\xi_0 E = 3.4 \pm 0.7$, and $E_2 = 36 \pm 13$ keV and this fit is shown in Figs. 5, 6, and 7. Table I lists the χ^2 for each fit. Table I also lists the parameters for the best possible fit to Aprile's data just to show how stable the fit parameters are. The best fit parameters represent only a modest change from the universal fit parameters and the fit is shown in Fig. 8. For all model fits, E_0 was fixed by the normalization of Eq. (9) and E_1 was fixed at 1 keV. If E_1 were allowed to vary, a broad range of values gives equally good χ^2 values, from 0.25 keV to 3 keV. A value of 1 keV was chosen because Rutherford scattering fails to describe the cross section at lower energies and it is reasonable that a δ electron of about 1 keV cannot make a charged blob; there are too few secondary electrons created to make a highly shielded, high charge-density region.

The value of E_2 required by the universal fit, 36 ± 13 keV, has great intuitive appeal. Figure 2 shows that the rate of energy loss below 50 keV increases dramatically. This is essential to forming a charged blob at the end of a track, but also the electron must scatter at large, random angles in order to ensure that it remains in a localized region. So we have calculated the angular distribution of electrons traversing a target of finite thickness using

TABLE I. The universal fit parameters used to draw the theoretical curves shown in Figs. 5, 6, and 7. The last line compares the best-fit parameters for Ref. 12 to the universal fit parameters.

Ref.	$\xi_1 E$	$\xi_0 E$	E_2	χ^2
25	0.337	3.37	36.3	1.37
26	0.337	3.37	36.3	2.85
12	0.337	3.37	36.3	2.21
12	0.217	3.37	40.8	0.68

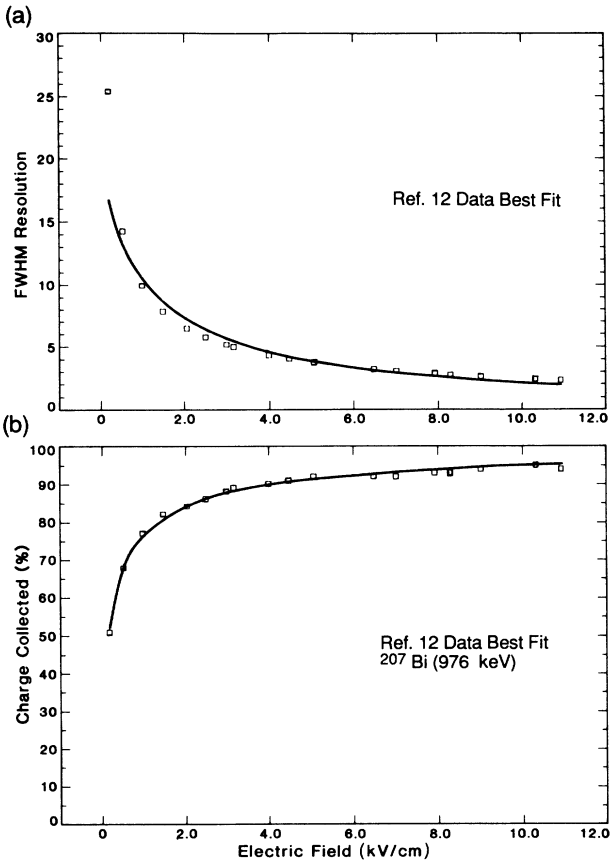

FIG. 8. For comparison to the unified fit, the best fit to the data in Ref. 12 is shown.

Moliere's scattering theory (which is best described by Bethe[27,16]). θ_{max} marks the peak in the angular distribution and it increases at lower energies, as we would expect. Assuming that the product of dE/dx and Θ_{max} is related to the probability of blob formation, we plot $\theta_{max} \times dE/dx$ in Fig. 9. It rises very rapidly at low energies and the range from 30-40 keV marks the transition from low probability to high probability.

Equations (11) and (13) can also be fit to charge collection and resolution data collected in liquid xenon. The best fit to our data[25] is shown in Fig.10. It is not obvious how to scale the parameters from argon to xenon and more data would be desirable to help understand the scaling mechanism. There are other xenon data sets in the literature[10,28] and the resolution has been measured at a few high field points[4,18] but these data are not as consistent as the argon data. In particular our resolution results in xenon are better than any of those quoted above.

III. CONCLUSIONS AND FUTURE DIRECTIONS

We have used a physically realistic model to show that there is a fundamental limit to the resolution that can be achieved in liquid argon. The limit is due to charge density fluctuations along an electron track and by the statistics of δ electron formation; both of which are fundamental properties of the material and cannot be avoided.

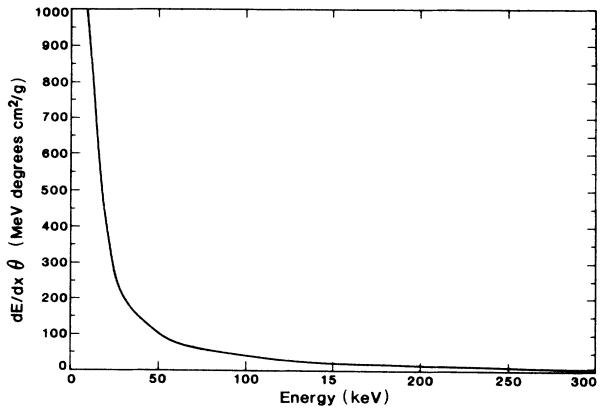

FIG. 9. The product of the average scattering angle and the rate of energy loss is related to the probability of "blob" formation at the end of an electron track. θ is the angle associated with the peak in the electron scattering angle distribution. The curve is the same for argon and xenon within the resolution of this figure.

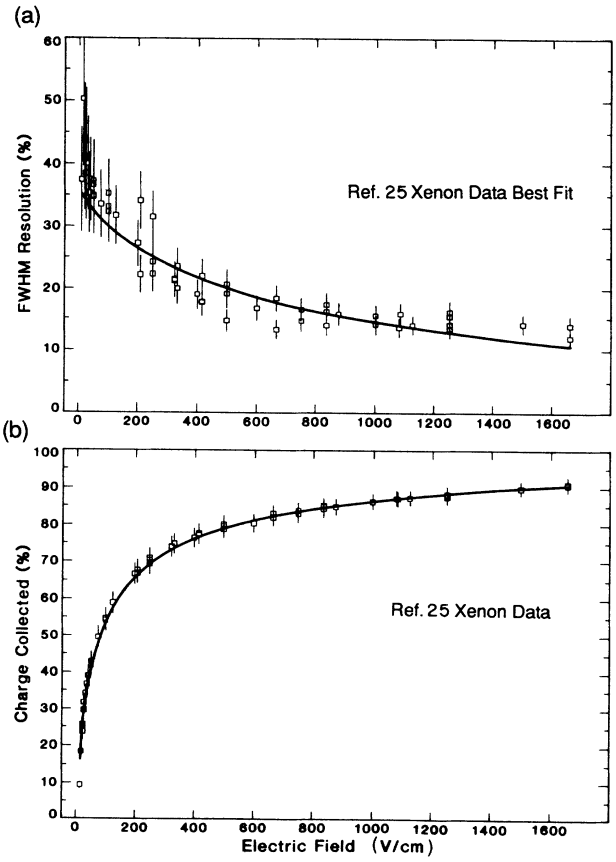

FIG. 10. A simultaneous fit of Eqs. (11) and (13) to the (a) energy resolution and (b) charge collected in liquid xenon using a 368-keV K shell conversion electron source. The best fit to these data requires $\xi_1 E = 0.128$, $\xi_0 E = 1.92$, and $E_2 = 51.0$ keV. E_1 was allowed to vary and the best value was 9.6 keV. The data shown here are from Ref. 25.

These limits are modeled by Eqs. (11) and (13) and they can be simplified for experimental analysis by noting that $a \approx 0.291 + 16.7/E_p$ and

$$\left[W_{\mathrm{FWHM}}(\%) \frac{E_c}{E_p} \right] = \frac{235.5}{\sqrt{E_p}} b \left[\frac{\ln(1+\xi_1)}{\xi_1} - \frac{\ln(1+\xi_0)}{\xi_0} \right],$$

where $b \approx [4.52 + (157/E_p)]^{1/2}$.

Similar fundamental limits exist in liquid xenon but the parameters in our model are not as well defined due to the limitations of the data.

The best way to improve the resolution of these detectors is to reduce ξ_0 and ξ_1. Since $\xi = N_0 \alpha / 4a^2 \mu\_E$, the simplest way to decrease ξ is to increase the electric field. Extrapolations of Figs. 5, 6, and 7 suggest that the fluctuations due to δ electrons will be equal to or smaller than the Fano factor fluctuations in argon only at 60 kV/cm. But this is impractical in experiments which require several centimeter drift distances.

A second approach would be to increase the electron-ion mobility. An order of magnitude estimate of what is required comes by noting that the relative electron-ion mobility in Ge is 50–100 times higher[29] than in argon and xenon, and Ge detectors do not appear to be limited by the statistics of the δ electrons. This suggests that adding methane to the xenon would not be sufficient since we only expect to increase the mobility by a factor of 2.[30] Similarly, changing to the solid phase should only increase the mobility by about a factor of two.[21] But we note that Cohen and Lekner[20] have shown that the low field electron mobility in argon varies as $T^{-3/2}$. Decreasing the temperature may give us the required factor of 50 increase in mobility if solid xenon was taken from its triple point to liquid-helium temperatures. There is experimental data[21] suggesting that the low field mobility varies as $T^{-3/2}$. But a possible complication is that the recombination coefficient α may be proportional to the electron mobility[2] and therefore the temperature dependence would cancel out of the problem. Obviously, this approach requires further work.

A third approach would be to lower the charge density along the electron track. N_0 is the charge per unit cell of dimension a. This could be decreased by increasing a (i.e. lowering the density of the liquid). Experiments above the critical point, near liquid densities, would be interesting. Especially since the value of ξ may depend nonlinearly on N_0/a^2 because a charge blob would have a highly screened region of charge at its center. The region below $\frac{1}{2}$ liquid density has been explored[22] with mixtures of hydrogen and xenon and the data supports these ideas.

A fourth approach to improving the resolution of liquid- and solid-Xe detectors would be to decrease the value of α. This is a phenomenological recombination coefficient that is derived from a simplified Langevin process.[2] It depends on inter-atomic potentials and other invariable quantities. But the effective recombination coefficient may be changed by doping the Ar or Xe with a photosensitive converter such as tetramethylamine or

tetraethylamine (TMA, TEA). Doke[8] has observed that when an electron recombines uv photons are emitted, and as the electric field is increased the light output decreases. A photosensitive dopant would absorb these photons and convert them back to electrons so that they could be used to compensate the ionization signal. This effect has already been seen for α particles in Xe doped with TEA (Ref. 31) and Ar doped with TMA (Ref. 32). These authors observed improved resolution, from 15% down to 4%, with the dopant and an α source but obtained no substantial improvement with an electron source. We are hopeful that further work will make it possible to achieve higher-energy resolution spectra for electrons.

ACKNOWLEDGMENTS

This work was supported in part by grants from the U.S. Department of Energy (No. DEAC-0381-ER40050) and The Presidents Fund at Caltech. We would like to acknowledge useful discussions with P. Doe and L. Varnell.

[1]L. Onsager, Phys. Rev. **54**, 554 (1938).
[2]H.A. Kramers, Physica **XVIII**, 665 (1952).
[3]G. Jaffe, Ann. Phys. **42**, 303 (1913).
[4]T. Takahashi *et al.*, Phys. Rev. A **12**, 1771 (1975).
[5]*Rare Gas Solids,* edited by M.L. Klein (Academic, London, 1977), Vol. II.
[6]U. Fano, Phys. Rev. **72**, 29 (1947).
[7]T. Doke *et al.*, Nucl. Instrum. Methods **134**, 353 (1976).
[8]T. Doke, Portugal. Phys. **12**, 9 (1981).
[9]M.D. Edmiston and C.R. Gruen, IEEE Trans. Nucl. Sci. **25**, 352 (1978).
[10]K. Masuda *et al.*, Nucl. Instrum. Methods **174**, 439 (1980).
[11]Th. Lindblad *et al.*, Nucl. Instrum. Methods **215**, 183 (1983).
[12]E. Aprile *et al.*, Nucl. Instrum. Methods **A261**, 519 (1987).
[13]P.J. Doe, H.-J. Mahler, and H.H. Chen, IEEE Trans. Nucl. Sci. **29**, 354 (1982).
[14]J. Thomas, in *Proceedings of the Conference on Low Level Counting and Liquid Drift Detectors,* edited by D. Cline (UCLA, Los Angeles, 1987).
[15]M.Z. Iqbal *et al.*, Nucl. Instrum. Methods **A259**, 459 (1987).
[16]M.Z. Iqbal, B.M.G. O'Callaghan, and H.T.-k Wong, Nucl. Instrum. Methods **A253**, 278 (1987).
[17]J. Thomas and D.A. Imel, Phys. Rev. A **36**, 614 (1987).
[18]I.M. Obodovskii and S.G. Pokachalov, Fiz. Nizk. Temp. **5**, 829 (1979) [Sov. J. Low Temp. Phys. **5**, 393 (1979)].
[19]J. Lekner, Phys. Rev. **158**, 130 (1967).
[20]M.H. Cohen and J. Lekner, Phys. Rev. **158**, 305 (1967).
[21]L.S. Miller, S. Howe, and W.E. Spear, Phys. Rev. **166**, 871 (1968).
[22]A.E. Bolotnikov *et al.*, Prib. Tekh. Eksp. **4**, 42 (1986) [Instrum. Exp. Tech. (USSR) Jan., 802 (1987)].
[23]D.M. Ritson, *Techniques of High Energy Physics* (Interscience, New York, 1961).
[24]L. Pages *et al.*, At. Data **4**, 1 (1972).
[25]D.A. Imel and J. Thomas, Nucl. Instrum. Methods (to be published).
[26]R.T. Scalettar *et al.*, Phys. Rev. A **25**, 2419 (1982).
[27]H.A. Bethe, Phys. Rev. **89**, 1256 (1952).
[28]A.S. Barabash *et al.*, Nucl. Instrum. Methods **A236**, 69 (1985).
[29]G.F. Knoll, *Radiation Detection and Measurement* (Wiley, New York, 1979).
[30]E. Shibamura, A. Hitachi, and T. Doke, Nucl. Instrum. Methods **131**, 249 (1975).
[31]S. Suzuki *et al.*, Nucl. Instrum. Methods **A245**, 366 (1986).
[32]D.F. Anderson, Nucl. Instrum. Methods **A242**, 254 (1986).

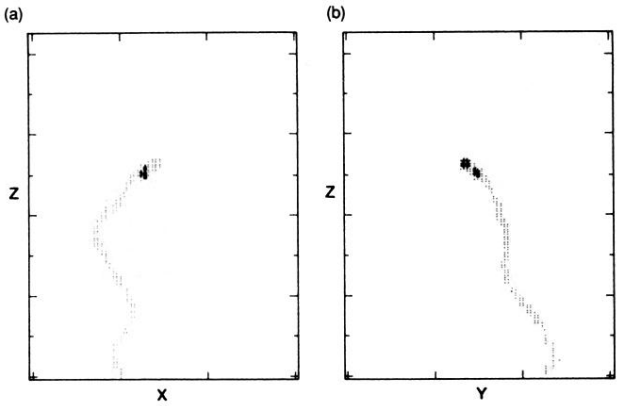

FIG. 1. (a) $X-Z$ and (b) $Y-Z$ projections of an electron track as it passes into a time projection chamber filled with 2 atmospheres of argon-methane (90/10 mixture). The electron stops near the center of the chamber and deposits 30-40 keV of energy in a well-localized "blob." The X and Y axes are 30 cm wide and the Z axis is scaled accordingly (see Ref. 15).